ELSEVIER

International Journal of Solids and Structures 41 (2004) 2551–2562

INTERNATIONAL JOURNAL OF SOLIDS and STRUCTURES

www.elsevier.com/locate/ijsolstr

On Saint-Venant's principle in the two-dimensional flexural vibrations of elastic beams

D.J. Foster *, V. Berdichevsky

Mechanical Engineering, Wayne State University, 7084 Lahser Rd., Bloomfield, Detroit, MI 48202, USA

Received 5 May 2003; received in revised form 12 November 2003

Abstract

In this paper we apply the method proposed in our previous paper [Int. J. Solids Struct. 40(13–14) (2003) 3293] to quantitatively estimate the violation of Saint-Venant's principle in the problem of flexural vibration of a two-dimensional strip. A probabilistic approach is used to determine the relative magnitude of the penetrating stress state and the results of computations are presented as a function of frequency. The results are not dependent on material properties except for Poisson's ratio. The numerical results given are appropriate for all isotropic materials with equal Lame' coefficients. Our major conclusion is that over a wide range of frequencies, the maximum propagating stress is always small compared with the maximum applied stress; hence Saint-Venant's principle may be said to apply in this problem. By considering applied loads with increasing spatial frequency content it was concluded that a smooth self-equilibrated load will cause a larger penetrating stress than a more irregular one. Although initially this may seem counter-intuitive, it results from the penetrating branch having the smoothest spatial distribution of all the branches of the solution to the dynamic elasticity equations. An interesting outcome of our study is that the accuracy of engineering theories for flexural vibrations is much higher than for longitudinal vibrations.

1. Introduction

For beams with a full cross-section, Barre' de Saint-Venant (1885) postulated that the stresses caused by a static self-equilibrating load are localized at the vicinity of the beam end, and form a "boundary layer". Neglecting the stress field caused by the self-equilibrating load reduces the study of the stress state away from the end to just the study of a two-dimensional elasticity problem on the cross-section. A detailed review of the subject was given in our previous paper, Berdichevsky and Foster (2003), together with a list of references to previously published work. In the case of a dynamic load, Lamb (1916) showed that a travelling wave is also excited, so that a self-equilibrated end load will cause some level of stress to penetrate into the beam: Saint-Venant's principle is violated. The above referenced paper proposed a method to characterize the level of the penetrating stress state, with particular reference to the symmetric axial load.

* Corresponding author. Tel.: +1-2486429404; fax: +1-2486420464.
E-mail address: dinver@sbcglobal.net (D.J. Foster).

0020-7683/$ - see front matter © 2003 Elsevier Ltd. All rights reserved.
doi:10.1016/j.ijsolstr.2003.12.007

We used an explicit solution of the elasticity equations in the form of a series, each term of the series being a partial solution; the first being the penetrating mode as constructed by Lamb (1916) and the remainder being decaying modes similar to those found for a static load. Any given load could, in principle, be constructed by the summation of these partial solutions multiplied by appropriate coefficients. Since the individual solutions are non-orthogonal, this turns out to be a tedious, approximate process. An alternative method to obtain a self-equilibrated load distribution using a finite number of partial solutions would be to assign values to all the series coefficients except for the coefficient of the penetrating mode, which would be determined by the requirement of zero resultant load. Moreover, since the self-equilibrated part of the end load would be different for each specific engineering problem, we needed a method to model many different types of spatial distributions. To accomplish this, the arbitrary coefficients for a particular analysis were selected from independent Gaussian distributions with zero mean and unit variance. Effectively, we treat the load as random, accept a probabilistic model for randomness and determine the probabilistic characteristics of the penetrating stress state. It is worth emphasizing that the actual load is not random, and that randomness only comes into play to model absence of our knowledge of the actual self-equilibrated part of the load. One may say that the information on the self-equilibrated part of the load is given in probabilistic terms, as a measure on the space of loads. In the paper referenced, this approach was used to study the errors of one-dimensional strip theories caused by the violation of Saint-Venant's principle in the case of longitudinal vibrations of elastic strips.

Herein, we apply this method to the problem of flexural vibrations of a semi-infinite elastic strip. We study the probabilistic characteristics of the penetrating solution. Our major conclusion is that over a wide range of frequencies, the maximum propagating stress is small compared with the maximum applied stress. Saint-Venant's principle may be said to apply in this problem, until the frequency approaches a critical high level. Below this frequency of vibration, the error involved is considerably smaller for flexural vibrations than it is for longitudinal vibrations.

The material is organized as follows. In the next section we give a necessary summary of the Lamb partial solutions for the semi-infinite strip, and construct the series expansion. In Section 3 the probabilistic model is introduced and the method of determining the penetrating stress state is outlined. The results of computations are presented in Section 4. The conclusions drawn from this study are given in Section 5, and an abbreviated list of references in section six (but see our previous paper for a more complete list of references).

2. Vibrations of a semi-infinite strip

Consider a semi-infinite strip of homogeneous isotropic material with Lame' elastic constants λ and μ and density ρ. It occupies the region $x \geqslant 0$, $-h \leqslant y \leqslant h$, unbounded in the direction z. The faces $y = h$, and $y = -h$ are free of traction; the end $x = 0$ is subjected to a load, which changes harmonically with time t at a frequency ω. The load causes normal stresses σ_{xx}, and σ_{yy} and shear stresses σ_{xy} with displacements u and v in the (x, y)-plane. The dynamic behavior is governed by

the momentum equation

$$\frac{\partial \sigma_{xx}}{\partial x} + \frac{\partial \sigma_{xy}}{\partial y} - \rho \frac{\partial^2 u}{\partial t^2} = 0, \quad \frac{\partial \sigma_{xy}}{\partial x} + \frac{\partial \sigma_{yy}}{\partial y} - \rho \frac{\partial^2 v}{\partial t^2} = 0 \tag{2.1}$$

the stress–strain relations

$$\sigma_{xx} = \lambda\left(\frac{\partial u}{\partial x} + \frac{\partial v}{\partial y}\right) + 2\mu \frac{\partial u}{\partial x}, \quad \sigma_{yy} = \lambda\left(\frac{\partial u}{\partial x} + \frac{\partial v}{\partial y}\right) + 2\mu \frac{\partial v}{\partial y}, \quad \sigma_{xy} = \lambda\left(\frac{\partial v}{\partial x} + \frac{\partial u}{\partial y}\right) \tag{2.2}$$

the free boundary conditions at the faces of the strip

$$\sigma_{yy} = 0, \quad \sigma_{xy} = 0 \quad \text{at } y = \pm h \tag{2.3}$$

and the boundary conditions at the strip edge

$$\sigma_{xx}(y,t) = f_{xx}(y)\cos\omega t + g_{xx}(y)\sin\omega t \tag{2.4}$$

$$\sigma_{xy}(y,t) = f_{xy}(y)\cos\omega t + g_{xy}(y)\sin\omega t \tag{2.5}$$

The functions $f_{xx}(y)$, $g_{xx}(y)$, $f_{xy}(y)$, and $g_{xy}(y)$ are assumed to be given. There is also a condition that there are no forces at infinity, which we formulate explicitly later.

Flexural vibrations correspond to functions $v(x,y,t)$ and $\sigma_{xy}(x,y,t)$ even in y and $u(x,y,t)$, $\sigma_{xx}(x,y,t)$ and $\sigma_{yy}(x,y,t)$ odd in y. Thus, $f_{xx}(y)$ and $g_{xx}(y)$ are odd functions of y while $f_{xy}(y)$, and $g_{xy}(y)$ are even functions.

The Lamb partial solutions are those solutions of 2.1 and 2.2 such that each unknown function has the form of a running wave; a function of y multiplied by $e^{i(kx-\omega t)}$. It is convenient to write the solutions in dimensionless form by introducing dimensionless stresses σ'_{xx}, σ'_{xy}, and σ'_{yy}, coordinates x', y', displacements u', v', frequency Ω, time t' and wave number k'

$$\sigma'_{xx} = \frac{\sigma_{xx}}{\mu}, \quad \sigma'_{xy} = \frac{\sigma_{xy}}{\mu}, \quad \sigma'_{yy} = \frac{\sigma_{yy}}{\mu}, \quad x' = \frac{x}{h}, \quad y' = \frac{y}{h}, \quad u' = \frac{u}{h}, \quad v' = \frac{v}{h} \tag{2.6}$$

$$\Omega^2 = \frac{\rho h\omega^2}{\mu}, \quad t' = \frac{t}{h}\sqrt{\frac{\mu}{\rho}} \quad \text{and } k' = \frac{k}{h} \tag{2.7}$$

In what follows we omit the primes.

The running wave solutions exist only for k and Ω linked by the dispersion equation

$$\frac{\tanh\beta}{\tanh\alpha} = \frac{(k^2+\beta^2)^2}{4k^2\alpha\beta} \tag{2.8}$$

where

$$\alpha^2 = k^2 - \frac{1-2\nu}{2-2\nu}\Omega^2, \quad \beta^2 = k^2 - \Omega^2 \tag{2.9}$$

Note that the right-hand side of the dispersion equation for the case of flexural vibrations is the inverse of that for longitudinal vibrations. The corresponding functions of y are

$$\begin{aligned}
u(y,k) &= \sinh\alpha y - \frac{(\beta^2+k^2)\sinh\alpha\sinh\beta y}{2k^2\sinh\beta}\\
v(y,k) &= \frac{2i\alpha k\cosh\alpha\cosh\beta y}{(\beta^2+k^2)\cosh\beta} - \frac{i\alpha}{k}\cosh\alpha y\\
\sigma_{xx}(y,k) &= \frac{i(k^2-\beta^2+2\alpha^2)\sinh\alpha y}{k} - i\frac{(\beta^2+k^2)\sinh\alpha\sinh\beta y}{k\sinh\beta}\\
\sigma_{yy}(y,k) &= -i(k^2+\beta^2)\left(\frac{\sinh\alpha y\sinh\beta - \sinh\alpha\sinh\beta y}{k\sinh\beta}\right)\\
\sigma_{xy}(y,k) &= -2\alpha\frac{\cosh\alpha\cosh\beta y - \cosh\alpha y\cosh\beta}{\cosh\beta}
\end{aligned} \tag{2.10}$$

We consider Ω as a given parameter and determine the wave numbers k as functions of the frequency Ω from the dispersion equation (2.8). The dispersion equation has one real root (designated as branch zero) but many complex roots. The first four branches are plotted in Fig. 1.

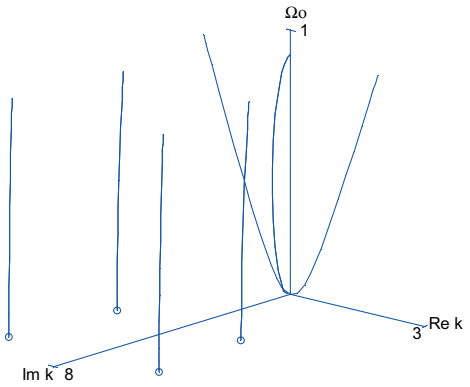

Fig. 1. Wave number k vs. frequency Ω_0 for branches 0–3.

For consistency with other authors, we plot the dimensionless frequency $\Omega_0 = h\omega\sqrt{\frac{\rho}{\lambda+2\mu}}$.

The branches shown correspond to the non-growing (away from the end) solutions, related to $\mathrm{Im}\,k \geqslant 0$. When computing quantities for branches with $\mathrm{Re}\,k < 0$ we replace k by its negative conjugate $-\bar{k}$. We will number all the branches for small Ω, attaching index 0 to the first penetrating branch, for which $\mathrm{Im}\,k = 0$ at all frequencies. For frequencies $\Omega_0 \leqslant 0.9068$ branch 1 has pure imaginary k. The values of $\mathrm{Im}\,k$ which start from zero at $\Omega_0 = 0$, remain small as the frequency increases and return to zero at $\Omega_0 = 0.9068$. Above this frequency, branch 1, like branch 0, has $\mathrm{Im}\,k = 0$ and is a penetrating branch. For the purpose of determining the possible magnitude of the dynamic penetrating stress state, branches zero and one are both treated as penetrating at all frequencies. Indices 2, 3, ... are given to branches with increasing k for $\mathrm{Re}\,k \geqslant 0$, and indices $\bar{2}, \bar{3}, \ldots$ to the corresponding branches with $\mathrm{Im}\,k \leqslant 0$. For the ath branch, k_a is a function of Ω. According to (2.9), α and β are also functions of Ω. For definiteness when determining α and

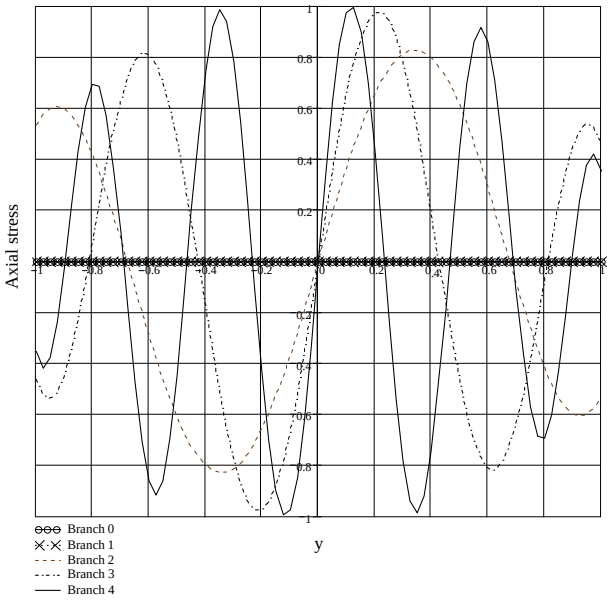

Fig. 2. Real part of normalized axial stress vs. distance across strip, for first five branches.

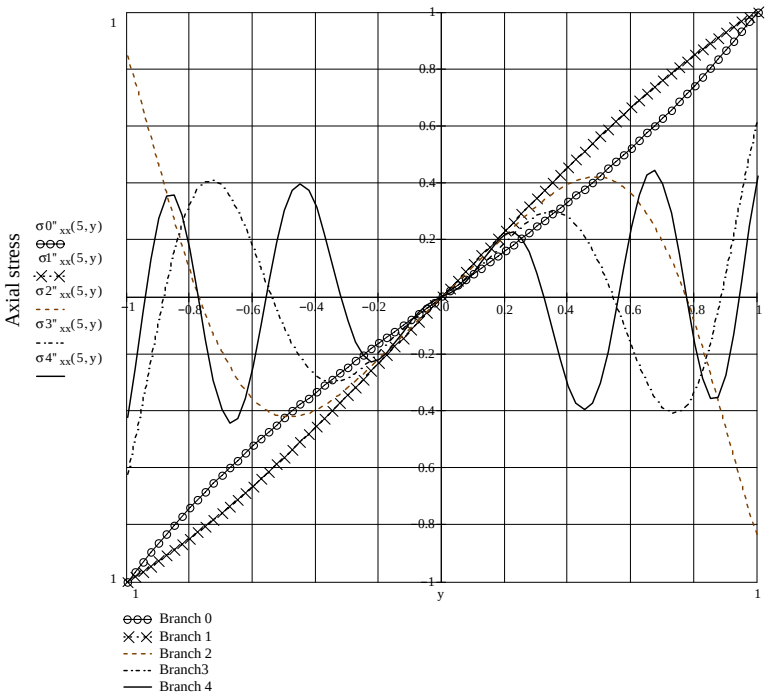

Fig. 3. Imaginary part of normalized axial stress vs. distance across strip, for first five branches.

β from (2.9) by the relations $\alpha^2 = k^2 - \frac{1-2v}{2-2v}\Omega^2$, $\beta^2 = k^2 - \Omega^2$, we choose the branch of the square root, which obeys the rule $\alpha(-\bar{k}, \Omega) = \bar{\alpha}(k, \Omega)$, $\beta(-\bar{k}, \Omega) = \bar{\beta}(k, \Omega)$.

Except for the special cases of branches zero and one, the ath branch has two real solutions, which are the real and imaginary parts (denoted by prime and double prime respectively) of the time dependent physical quantities. For the axial displacement, for example, these are denoted by $u'(x, y, t)$ and $u''(x, y, t)$. They are derived from the fundamental solution (2.10) and the equation

$$u(x, y, t, k_a) = u(y, k_a)\mathrm{e}^{\mathrm{i}(k_a x - \Omega t)} = u'_a(x, y, t) + \mathrm{i}u''_a(x, y, t) \tag{2.11}$$

Similarly

$$\begin{aligned}
v(x, y, t, k_a) &= v(y, k_a)\mathrm{e}^{\mathrm{i}(k_a x - \Omega t)} = v'_a(x, y, t) + \mathrm{i}v''_a(x, y, t)\\
\sigma_{xx}(x, y, t, k_a) &= \sigma_{xx}(y, k_a)\mathrm{e}^{\mathrm{i}(k_a x - \Omega t)} = \sigma'_{xx,a}(x, y, t) + \mathrm{i}\sigma''_{xx,a}(x, y, t)\\
\sigma_{yy}(x, y, t, k_a) &= \sigma_{yy}(y, k_a)\mathrm{e}^{\mathrm{i}(k_a x - \Omega t)} = \sigma'_{yy,a}(x, y, t) + \mathrm{i}\sigma''_{yy,a}(x, y, t)\\
\sigma_{xy}(x, y, t, k_a) &= \sigma_{xy}(y, k_a)\mathrm{e}^{\mathrm{i}(k_a x - \Omega t)} = \sigma'_{xy,a}(x, y, t) + \mathrm{i}\sigma''_{xy,a}(x, y, t)
\end{aligned} \tag{2.12}$$

From (2.11), the axial displacement components are

$$\begin{aligned}
u'_a(x, y, t) &= (u'(y, k_a)\cos(k'_a x - \Omega t) - u''(y, k_a)\sin(k'_a x - \Omega t))\mathrm{e}^{-k''_a x}\\
u''_a(x, y, t) &= (u'(y, k_a)\sin(k'_a x - \Omega t) + u''(y, k_a)\cos(k'_a x - \Omega t))\mathrm{e}^{-k''_a x}
\end{aligned} \tag{2.13}$$

Similar formulas for the other physical quantities follow from (2.11). For the branches associated with the conjugate roots of the dispersion equation $-\bar{k}$, we have $u(-\bar{k}, \Omega) = \bar{u}(k, \Omega)$, $v(-\bar{k}, \Omega) = \bar{v}(k, \Omega)$. Therefore

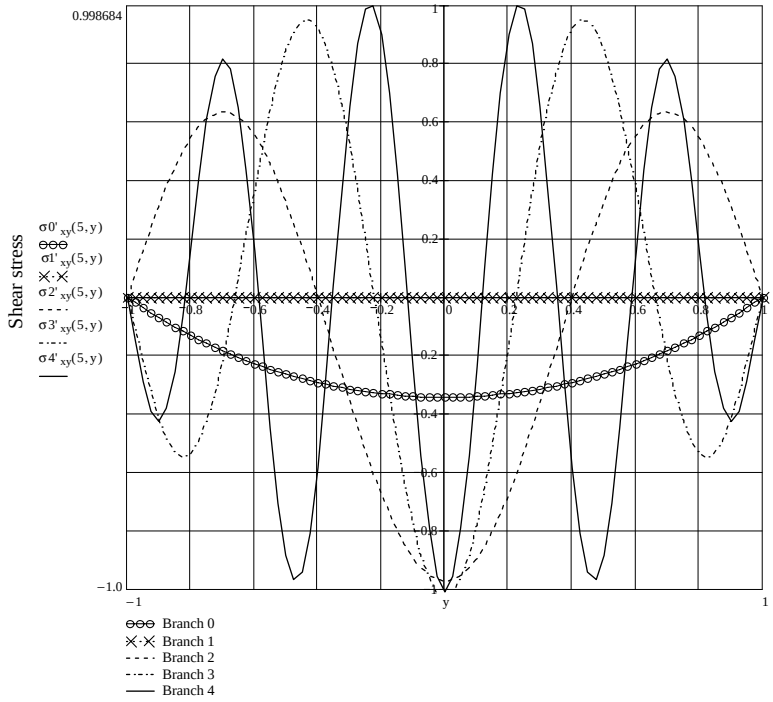

Fig. 4. Real part of normalized shear stress vs. distance across strip, for first five branches.

$$\begin{aligned} u'_a(x,y,t) &= (u'(y,k_a)\cos(k'_a x+\Omega t) - u''(y,k_a)\sin(k'_a x+\Omega t))\mathrm{e}^{-k''_a x} \\ u''_a(x,y,t) &= (-u'(y,k_a)\sin(k'_a x+\Omega t) - u''(y,k_a)\cos(k'_a x+\Omega t))\mathrm{e}^{-k''_a x} \end{aligned} \tag{2.14}$$

Again, similar formulas for the other physical quantities follow from (2.11). So, we have, for each branch with complex values for k, four independent real solutions.

For branch zero, there are two penetrating branches with real wave numbers k and $-k$. They correspond to the waves running to the right and left, respectively. We assume that here are no waves coming from infinity. Thus only the penetrating branch with positive k should be taken into account. It generates two real independent solutions. It is easy to see that for small values of Ω, α is real while β is pure imaginary. Thus, for the penetrating branch zero $u''(y,k_0) = v'(y,k_0) = \sigma'_{xx}(y,k_0) = \sigma'_{yy}(y,k_0) = \sigma''_{xy}(y,k_0) = 0$ and simlarly for the lightly damped branch one, we find $u'(y,k_1) = v'(y,k_1) = \sigma'_{xx}(y,k_1) = \sigma'_{yy}(y,k_1) = \sigma'_{xy}(y,k_1) = 0$.

The two real independent solutions for the propagating longitudinal displacements are

$$\begin{aligned} u'_0(x,y,t) &= u'(y,k_0)\cos(k'_0 x-\Omega t) \\ u''_0(x,y,t) &= u'(y,k_0)\sin(k'_0 x-\Omega t) \end{aligned} \tag{2.15}$$

For each value of Ω, we may seek the solution of the boundary value problem in the form of series with respect to the obtained partial solutions. For example, for the axial component of displacements one can write

$$\begin{aligned} u(x,y,t) = {} & A_0 u'(y,k_0)\cos(k'_0 x-\Omega t) + B_0 u'(y,k_0)\sin(k'_0 x-\Omega t) + \sum_{a=1}^{\infty} A_a u'_a(x,y,t) + B_a u''_a(x,y,t) \\ & + \sum_{a=1}^{\infty} C_a u'_a(x,y,t) + D_a u''_a(x,y,t) \end{aligned} \tag{2.16}$$

At the edge $x = 0$, using (2.13)–(2.15), and noting that since $u'(y, k_1) = 0$ we can make the change of notation A_1 for $A_1 - C_1$ and B_1 for $B_1 - D_1$, this becomes

$$\begin{aligned} u(x,y,t) &= A_0 u'(y,k_0)\cos\Omega t - B_0 u'(y,k_0)\sin\Omega t + A_1 u''(y,k_1)\sin\Omega t + B_1 u''(y,k_1)\cos\Omega t \\ &+ \sum_{a=2}^{\infty}((A_a + C_a)u'(y,k_a) + (B_a - D_a)u''(y,k_a))\cos\Omega t \\ &+ \sum_{a=2}^{\infty}((A_a - C_a)u''(y,k_a) - (B_a + D_a)u'(y,k_a))\sin\Omega t \end{aligned} \tag{2.17}$$

Similar formulas and expansions hold for the other fields.

The coefficients A_0, B_0, A_1, B_1, A_a, B_a, C_a, D_a should be found from the boundary conditions (2.4) and (2.5). Let us write down these conditions explicitly in terms of the unknown coefficients

$$\begin{aligned} &B_0\sigma''_{xx}(y,k_0) + B_1\sigma''_{xx}(y,k_1) + \sum_{a=2}^{\infty}((A_a + C_a)\sigma'_{xx}(y,k_a) + (B_a - D_a)\sigma''_{xx}(y,k_a)) = f_{xx}(y) \\ &A_0\sigma''_{xx}(y,k_0) + A_1\sigma''_{xx}(y,k_1) + \sum_{a=2}^{\infty}((A_a - C_a)\sigma''_{xx}(y,k_a) - (B_a + D_a)\sigma'_{xx}(y,k_a)) = g_{xx}(y) \\ &A_0\sigma'_{xy}(y,k_0) + B_1\sigma''_{xy}(y,k_1) + \sum_{a=2}^{\infty}((A_a + C_a)\sigma'_{xy}(y,k_a) + (B_a - D_a)\sigma''_{xy}(y,k_a)) = f_{xy}(y) \\ &-B_0\sigma'_{xy}(y,k_0) + A_1\sigma''_{xy}(y,k_1) + \sum_{a=2}^{\infty}((A_a - C_a)\sigma''_{xy}(y,k_a) - (B_a + D_a)\sigma'_{xy}(y,k_a)) = g_{xy}(y) \end{aligned} \tag{2.18}$$

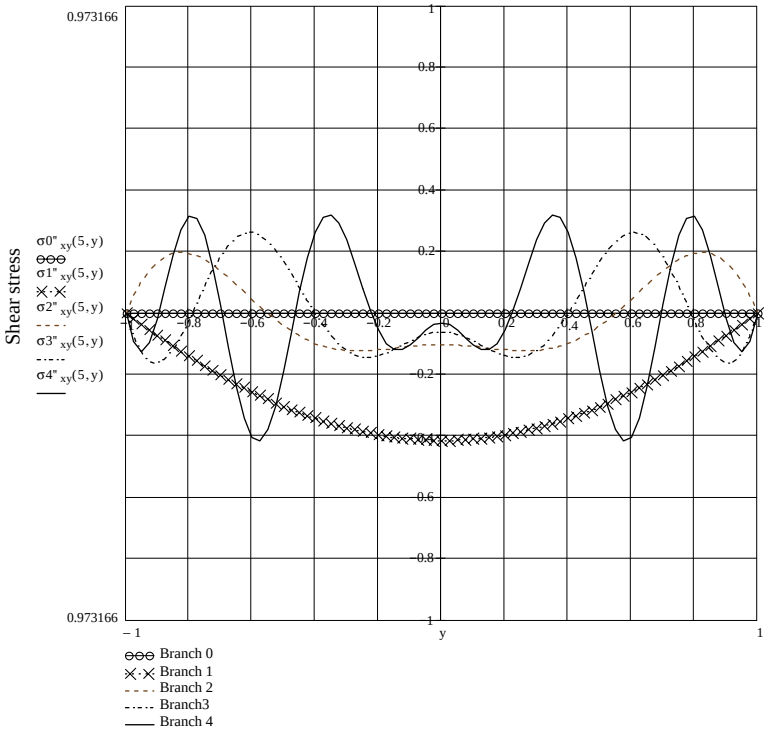

Fig. 5. Imaginary part of normalized shear stress vs. distance across strip, for first five branches.

The penetrating stress for the given applied load may be computed from (2.18) by determining the coefficients A_0 and B_0. The basic functions in this expansion, $\sigma'_{xx}(y,k_a)$, $\sigma''_{xx}(y,k_a)$, $\sigma'_{xy}(y,k_a)$ and $\sigma''_{xy}(y,k_a)$ look, to some extent, similar to the basic functions of a Fourier series. They are shown for each of the first five branches, in Figs. 2–5, for a frequency $\Omega_0 = 0.3$. At this frequency, the associated values of k are

Branch	Real k	Imaginary k
0	0.875	0.0
1	0.0	0.595
2	1.387	3.724
3	1.677	6.937
4	1.992	13.271

3. Probabilistic model

We intend to find from the system of equation (2.18) the coefficients A_0 and B_0 that specify the magnitude of the penetrating stress state. We assume that the load is self-equilibrated. Due to the antisymmetric properties of the problem, for a self-equilibrated shear load and moment of the (inherently self-equilibrated) axial load, functions $f_{xx}(y)$, $g_{xx}(y)$, $f_{xy}(y)$ and $g_{xy}(y)$ must obey the conditions

$$\int_{-1}^{1} f_{xx}(y)y\,\mathrm{d}y = \int_{-1}^{1} g_{xx}(y)y\,\mathrm{d}y = \int_{-1}^{1} f_{xy}(y)\,\mathrm{d}y = \int_{-1}^{1} g_{xy}(y)\,\mathrm{d}y = 0 \tag{3.1}$$

Absence of knowledge of $f_{xx}(y)$, $g_{xx}(y)$, $f_{xy}(y)$ and $g_{xy}(y)$ corresponds to the absence of knowledge of the coefficients A_a, B_a, C_a and D_a. Therefore, instead of prescribing a probabilistic model for $f_{xx}(y)$, $g_{xx}(y)$, $f_{xy}(y)$ and $g_{xy}(y)$, one can give a probabilistic model for the coefficients A_a, B_a, C_a and D_a. We assume in what follows that these coefficients are independent Gaussian random variables with zero mean and unit variances. Then the coefficients A_0, B_0, A_1 and B_1 determined from (3.1) as linear functions of A_a, B_a, C_a and D_a are also Gaussian variables with zero mean.

The degree to which Saint-Venant's principle is violated may be characterized by the ratio θ of the maximum penetrating stress to the maximum value of the stress at the loaded end

$$\theta = \frac{\sqrt{A_0^2 + B_0^2}\max\limits_y \sqrt{\sigma''_{xx}(y,k_0)^2 + 2\sigma'_{xy}(y,k_0)^2 + \sigma''_{yy}(y,k_0)^2}}{\max\limits_y \sqrt{f_{xx}(y)^2 + f_{xx}(y)^2 + 2f_{xy}(y)^2 + 2g_{xy}(y)^2 + f_{yy}(y)^2 + g_{yy}(y)^2}} \tag{3.2}$$

where $f_{yy}(y)\cos\Omega t + g_{yy}(y)\sin\Omega t$ is the yy-component of the stress tensor at $x = 0$. If the self-equilibrated load at the beam end is of the same order as the non-equilibrated one then θ may serve as a measure of the error induced by using Saint-Venant's principle in dynamical problems.

4. Results

Ratio θ is a random variable. Its properties were determined numerically by running a Monte-Carlo analysis, where for each of 250 calculation the coefficients A_a, B_a, C_a and D_a were randomly selected from a set of Gaussian variables with zero mean and variance of unity. Initially, calculations were made for the two cases of including either three or six branches. We observed that, as in the case of longitudinal vibrations,

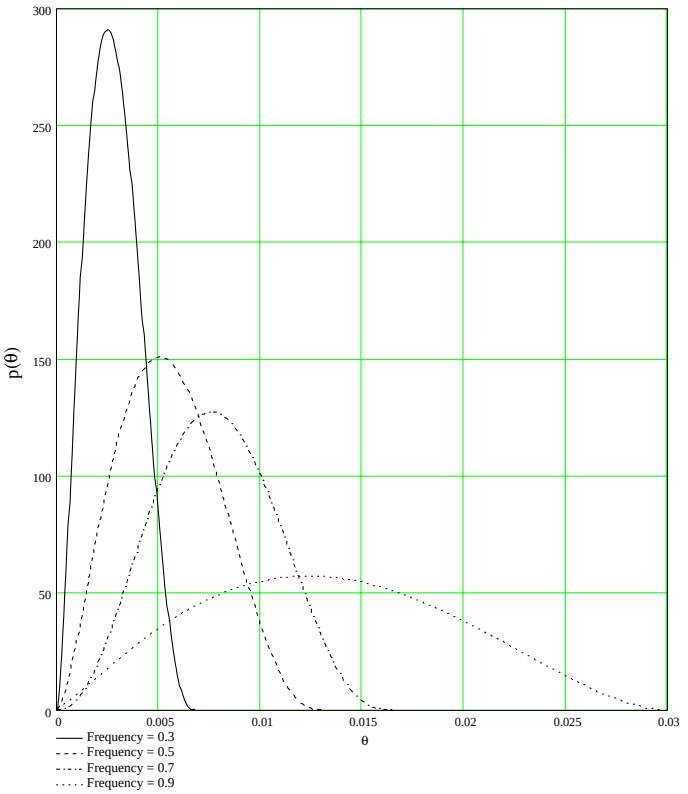

Fig. 6. Probability density function for the ratio θ at four frequencies, for the smoothest distribution.

the beta distribution provides a good description of the histogram of the numerical results. The beta distribution has a probability density given by

$$p(x) = \left\{ \begin{array}{ll} \frac{1}{B(a,b)} x^{a-1}(1-x)^{b-1} & 0 \leqslant x \leqslant 1 \\ 0 & \text{otherwise} \end{array} \right\}, \quad B(a,b) = \frac{\Gamma(a)\Gamma(b)}{\Gamma(a+b)} \tag{4.1}$$

For a random variable defined on some finite interval $[0, d]$ the beta distribution should be scaled accordingly. The probability density function $p(\theta)$ of the ratio θ is shown in Fig. 6 for the values of frequency $\Omega_0 = 0.3$, 0.5, 0.7 and 0.9 (three branches beyond the penetrating one were involved in these computations). In this figure we plot the beta distributions fitted to the histograms of the computed ratios.

The computed values for the parameters a and b were nearly constant across all frequencies where $\Omega_0 \leqslant 0.9$, with $1.8 < a < 2.5$ and $3.4 < b < 4.5$. The increase in the average value $\bar{\theta}$ is mostly due to the increase in the parameter d and is shown as a function of frequency in Fig. 7. We see from Fig. 7 that the Saint-Venant principle produces average errors less than 1.5% if the frequency $\Omega_0 \leqslant 0.9$. Note that this is an average estimate: in fact, errors may be as large as 3% for a smooth load distribution, as follows from the probability distributions shown in Fig. 6.

Integrating the probability density function $p(\theta)$ up to a certain given value Θ, one determines the probability $P(\Theta)$ that error Θ does occur. Subtracting this value from unity gives the probability $Q(\Theta) = 1 - P(\Theta)$ that the error exceeds the certain value Θ. A graph of $Q(\Theta)$ is given in Fig. 8 for the frequencies $\Omega_0 = 0.1$, 0.3, 0.5, 0.7 and 0.9. From these graphs we see that the probability of the error being greater than 1.5% (i.e. $\Theta = 0.015$) was 0.4 for a frequency $\Omega_0 = 0.9$ but is near zero for $\Omega_0 \leqslant 0.7$.

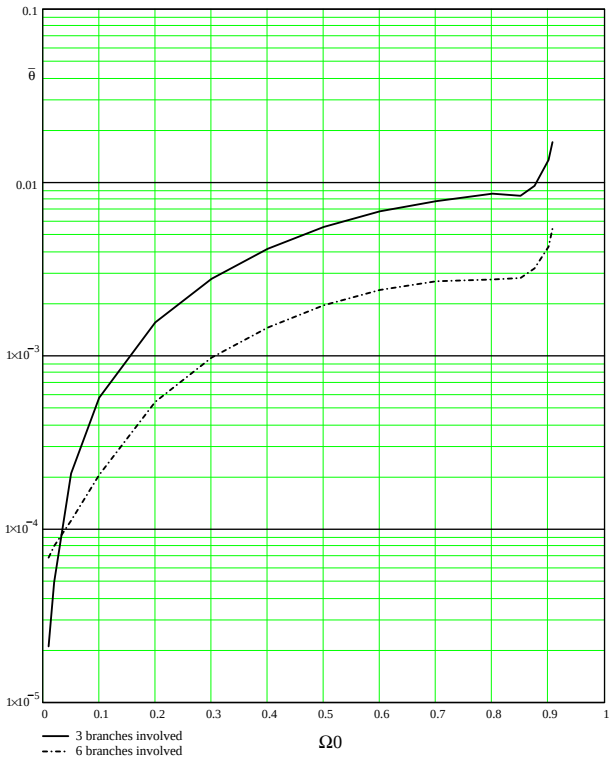

Fig. 7. Mean value of θ vs. frequency Ω_0 for the case of three branches and six branches involved.

From the numerical simulation we found that the presence of the higher harmonics of the self-equilibrated load distribution, associated with higher mode numbers, caused a reduction of the ratio θ. To obtain information on the effect of the number of branches, computations of the ratio for the case of A_a, B_a, C_a and D_a being Gaussian variables with zero mean, for $2 \leqslant a \leqslant 11$ (i.e. from 3 to 12 branches including the penetrating branches) were made. The results of the calculations of the probability density function for the inclusion of 3, 4, 5, 6 and 7 branches is given in Fig. 9 for a frequency $\Omega_0 = 0.5$. The corresponding plot of the mean value of the ratio is given in Fig. 10; it shows that θ decreases as the number of branches included increases from 3 to 12. From this, it was expected that a smooth self-equilibrated load would cause a larger penetrating stress than a highly irregular one.

5. Conclusions

A probabilistic approach was used to determine the relative magnitude of the penetrating stress state resulting from dynamic self-equilibrating anti-symmetric loads, as functions of the frequency of loading and the distribution shape. The computing power of readily available digital computers make direct application of 'Monte-Carlo' solution methods a practical way to use a probabilistic approach for loosely defined loading conditions. The results are not dependent on material properties except for Poisson's ratio. The numerical results given are appropriate for all isotropic materials with equal Lame' coefficients. Over a wide range of frequencies, the maximum propagating stress is always small compared with the maximum applied stress. Saint-Venant's principle may be said to apply in this problem, until the frequency approaches a

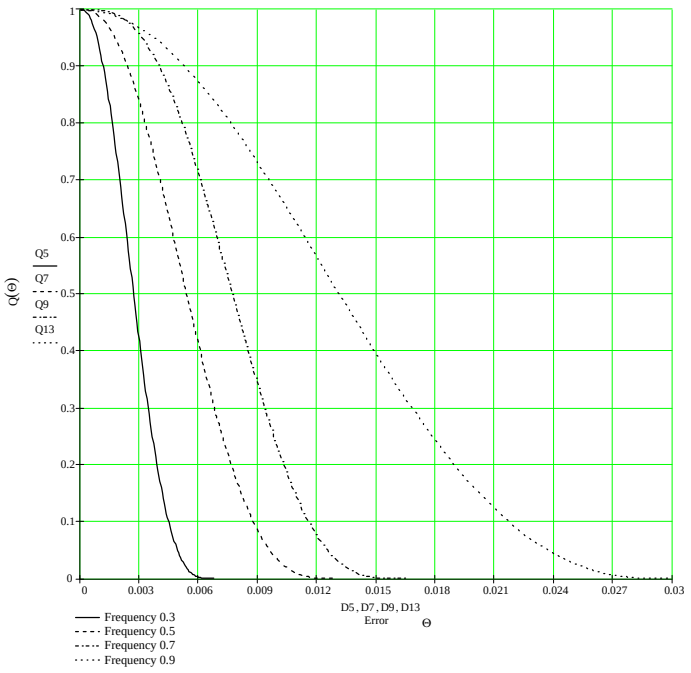

Fig. 8. Probability $Q(\Theta)$ that the ratio θ exceeds the value Θ at four frequencies when three branches are involved.

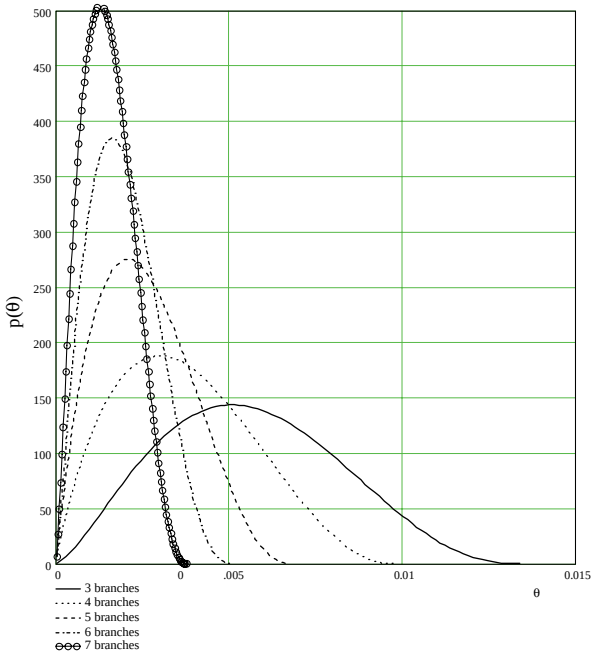

Fig. 9. Change in the probability density function $p(\theta)$ with increase in the number of branches involved at a frequency $\Omega_0 = 0.5$.

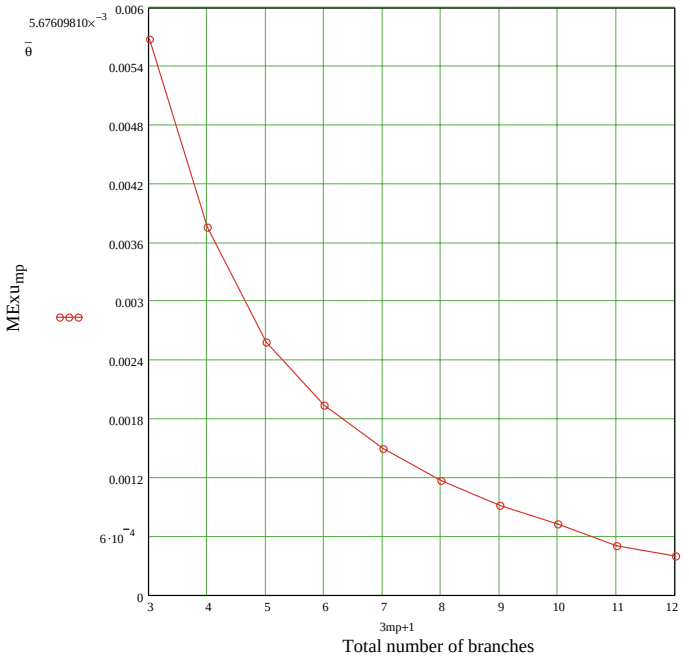

Fig. 10. Effect of increasing the number of branches involved on the mean value of θ at a frequency $\Omega_0 = 0.5$.

critical high level. By considering applied loads with increasing spatial frequency content it was concluded that a smooth self-equilibrated load will cause a larger penetrating stress than a more irregular one. Although initially this may seem counter-intuitive, it results from the penetrating branch having the smoothest spatial distribution of all the branches of the solution to the dynamic elasticity equations. An interesting outcome of our study is that the accuracy of engineering theories for flexural vibrations is much higher than for longitudinal vibrations.

References

Barre' de Saint-Venant, A.J.C., 1885. Memoir sur la torsion des prismes. Mem. Divers Savants 1.

Berdichevsky, V., Foster, D., 2003. On Saint-Venant's principle in the dynamics of elastic beams. Int. J. Solids Struct. 40 (13–14), 3293–3310.

Lamb, H., 1916. On waves in an elastic plate. Proc. R. Soc. London, Ser. A 93, 114–128.